

NUMERICAL MODELS OF BLACK HOLE ACCRETION FLOWS

CHARLES F. GAMMIE

*Loomis Laboratory of Physics, 1110 West Green Street, Urbana, IL 61801;
gammie@uiuc.edu*

JONATHAN C. MCKINNEY

*Center for Astrophysics, MS-51, 60 Garden Street, Cambridge, MA 02138;
mckinney@cfa.harvard.edu*

Active galactic nuclei, black hole binaries, and gamma-ray bursts are all probably powered by an accretion flow around a rotating black hole. It has recently become possible to construct numerical, fully relativistic ideal MHD models of these flows. The current generation of codes has undergone extensive testing and, remarkably, quite different codes produce quantitatively consistent results. Numerical models of thick, nonradiative accretion flows show that the matter accreted onto the black hole has smaller specific angular momentum per baryon than anticipated in the classical thin disk model. If supermassive black holes acquire their mass through a similar series of accretion flows, then they should reach spin equilibrium at $a/M \sim 0.93$, much less than the 0.998 envisioned in classical disk theory. Numerical models also show low density regions over the poles of the black hole. These regions are approximately force-free, and the electromagnetic field structure there is consistent with the Blandford-Znajek force-free magnetosphere model.

1. INTRODUCTION

Black hole accretion flows are believed to lie at the heart of some of the most luminous objects in the universe, including active galactic nuclei (AGN), black hole binaries, and gamma-ray bursts. The putative black holes in these systems span almost nine orders of magnitude in mass, from $3 \times 10^9 M_\odot$ in galactic nuclei to $\sim 10 M_\odot$ in black hole binaries. One might think that systems with such different mass, length, and time scales would *look* very different. But AGNs and black hole binaries exhibit remarkable similarities, including broad Fe K α line emission and superluminal jets. This is surprising. It suggests that there are some universal aspects to black hole accretion flows. Perhaps the gross features of these systems

are set by simple dynamical ingredients: the presence of strong gravity, rotation, and electromagnetic fields.

This possibility motivates the study of numerical, scale-free, nonradiative, models for black hole accretion flow. This is the subject of this contribution. One shouldn't take these nonradiative models too seriously (they are, after all, invisible!), but they provide a dynamical foundation for the more sophisticated models that will surely follow.

2. CLASSICAL DISK AND MAGNETOSPHERE MODELS

Our intuition about black hole accretion flows is informed mainly by two well-known models: the thin disk^{1,2,3,4,5}, and the force-free magnetosphere⁶. Here we will give an abbreviated summary of these models to set the stage for our numerical results.

2.1. THIN DISK

In the thin disk model the plasma orbits on circular, equatorial geodesics, gradually losing angular momentum and energy as it spirals in toward the black hole.^a The properties of circular equatorial geodesics are analytic, although the resulting expressions are complicated¹⁰.

The thin disk extends inward from large distance to the innermost stable circular orbit (ISCO). The plasma then falls gently into the black hole, retaining the energy and angular momentum it had on the ISCO. Table 1 gives the location of the ISCO for a few representative values of a/M (negative values indicate a counterrotating disk).

The luminosity of the thin disk is whatever energy each baryon had to give up on its way to the last stable orbit:

$$L_{acc} = (1 + u_{t,ISCO})\dot{M}_o c^2 = \epsilon \dot{M}_o c^2 \quad (1)$$

where \dot{M}_o is the rest-mass accretion rate, and ϵ is the "accretion efficiency," i.e. what fraction of c^2 per gram of accreted rest-mass is liberated as radiative energy. ϵ depends only on a/M and varies between 0.05 and 0.42.

^aNonequatorial disks would result from the infall of matter at large radius with angular momentum misaligned with the black hole spin. The Bardeen-Petterson effect^{7,8,9}, however, is expected to force a thin disk into the equatorial plane of a rotating black hole at $\sim 10^2 M$.

Bardeen¹ pointed out that under the above assumptions an initially nonrotating hole would reach maximal spin in finite time. This excited considerable astrophysical interest in rotating holes.

Thorne¹¹, in an important amendment to Bardeen's result, noted that if the photons radiated from the disk surface are isotropic in the rest frame of the plasma then some are inevitably captured by the black hole. Captured photons tend to have lower specific angular momentum than escaping photons. A detailed calculation shows that the thin disk will bring the black hole into spin equilibrium at $a/M = 0.998$. This is not a trivial difference; the 0.2% reduction in a/M reduces ϵ from 0.42 to 0.32. Thorne also notes in passing that magnetic fields may change the efficiency of the flow by connecting the disk to the plasma in the plunging region.

a/M	r_{ISCO}	u_ϕ	$-u_t$	ϵ
-1	9	$22/(3\sqrt{3})$	$11/(3\sqrt{15})$	0.053
-0.9	8.72	4.17	0.946	0.054
0	6	$2\sqrt{3}$	$2\sqrt{2}/3$	0.057
0.9	2.32	2.10	0.844	0.156
1	1	$2/\sqrt{3}$	$1/\sqrt{3}$	0.422

One can of course go beyond these basic results and calculate the internal structure of the disk using the α disk formalism (e.g. the model of Shakura & Sunyaev⁴), with the famous result that disks accreting near the Eddington limit are radiation dominated, unstable, and therefore (at least in the α theory) not self-consistent. The α disk models also indicate that the disk becomes thicker and approach $H/R \sim 1$ near the Eddington limit.

2.2. FORCE-FREE MAGNETOSPHERE

It is plausible that the region outside a thin disk contains a magnetic field (trapped by the disk) and a tenuous plasma. If the black hole is not rotating, then a steady approximate solution for the field is just a split monopole: $B^r = C/r^2$ above the disk and $-C/r^2$ below.^b The field is time steady and carries no energy or angular momentum. But what would happen if the black hole were spun up? The initially nonrotating field lines would be "attached" to a rotating black hole at the horizon and to a nonrotating

^bHere $B^r = {}^*F^{tr}$ in Boyer-Lindquist coordinates, where *F is the dual of the electromagnetic field tensor.

plasma at large r . Would energy and angular momentum then flow along the field lines?

This is the question considered by Blandford & Znajek (BZ) ⁶, who solved for the structure of a force-free magnetosphere in the slow rotation ($a/M \ll 1$) limit. Force-free here means that the $\mathbf{J} \times \mathbf{B}$ force (rewritten $J_\mu F^{\mu\nu}$) vanishes. This is equivalent to ideal MHD in the limit of vanishing plasma density and pressure. Using a monopolar field as a zeroth order solution BZ obtain the solution for a rotating hole to lowest nontrivial order in a/M . From this it is possible to calculate the energy flux on the event horizon, which is nonvanishing and *outward*. So energy does flow out along the field lines, and energy can be removed from a black hole by a tenuous axisymmetric plasma!

The BZ luminosity is

$$L_{BZ} = \frac{2\pi}{3} \left(\frac{a}{M}\right)^2 (B_H^r)^2 \left(\frac{GM}{c^2}\right)^2 c + O\left(\left(\frac{a}{M}\right)^4\right), \quad (2)$$

where B_H^r is the radial component of the field strength on the horizon in the Boyer-Lindquist frame. Then $L_{BZ}/L_{acc} \sim 1$ if the rest-mass energy density on the horizon is of order the magnetic energy density, although there are possibly large dimensionless factors that must be evaluated to obtain a more precise estimate.

2.3. BLACK HOLES IN NATURE

The real situation is, of course, quite a bit more complicated than these simple models. Figure 1 shows a cartoon of what we imagine a black hole accretion flow really looks like. The cartoon includes a possibly warped, centrifugally supported disk surrounded by a corona. The reader is free to mentally vary the ratio of disk-to-corona, possibly setting the disk component to zero. Magnetic field lines thread the disk, and a turbulent field is tangled in the disk. Field lines connect the disk and hole through the plunging region. The ratio of mean to tangled field is as yet unknown. A wind or jet is launched somewhere in the immediate neighborhood of the hole, although it may be launched directly along field lines that thread the hole through a Blandford-Znajek process, or along field lines that thread the inner disk. The inner disk itself is likely to be radiation dominated if the flow is optically thick.

All of the above structures are likely to be time-variable, with turbulence in the disk driven by the unavoidable magnetorotational instability

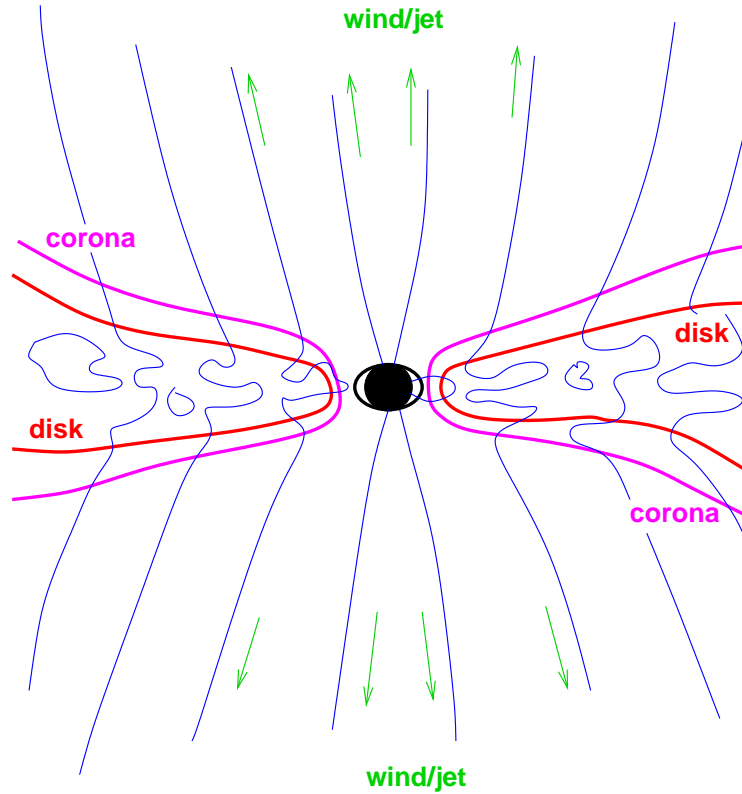


Figure 1. The circumbathic plasma.

¹³. Time-steady models may however capture some aspects of the time-averaged flow.

3. GRMHD

The preceding discussion motivates the development of numerical models for black hole accretion flows. Does a self-consistent, time-dependent model match the thin disk predictions for the angular momentum and energy of the accreted plasma? And what is the relative importance of the Blandford-Znajek effect? As a first effort to answer these questions we will consider nonradiative, axisymmetric models for the plasma using the MHD approximation.

Compared to the more familiar nonrelativistic MHD, there are two new

physical ideas in GRMHD: the incorporation of special relativistic effects such as the inertia of the field (which limits the wave speeds to the speed of light), and the treatment of the background geometry. Komissarov¹² provides a clear introduction to special relativistic MHD, although the basic ideas have been known since the work of Lichnerowicz¹⁴ and others¹⁵.

In moving from nonrelativistic MHD to relativistic MHD, the first step is to define an appropriate set of variables to describe the fluid. We begin by replacing the nonrelativistic density ρ with the rest-mass density $\rho_o = nm$, where n is the particle number density and m the mean mass per particle. The internal energy u and pressure p are scalars measured in the rest frame of the fluid and remain well defined. We replace the three-velocity \mathbf{v} with the four-velocity \mathbf{u} (and the normalization condition $u_\alpha u^\alpha = -1$). Finally, the magnetic field continues to have three degrees of freedom which can be represented either by $B^i = {}^*F^{it}$ or by the four-vector $b^\mu = {}^*F^{\mu\nu} u_\nu$, which evidently satisfies the condition $b_\mu u^\mu = 0$.

We are now equipped to write down the governing equations; we assume a coordinate basis. First, conservation of particle number:

$$\partial_t(\sqrt{-g}\rho_o u^t) = -\partial_i(\sqrt{-g}\rho_o u^i) \quad \partial_t\rho = -\nabla \cdot (\rho\mathbf{v}). \quad (3)$$

The expression on the right is the nonrelativistic counterpart. This is an *approximation* in the sense that it ignores particle creation and destruction processes. Here $\sqrt{-g}$ is the determinant of the metric; for the Kerr metric in Boyer-Lindquist or Kerr-Schild coordinates, $\sqrt{-g} = (r^2 + a^2 \cos^2\theta) \sin\theta$.

We also adopt the MHD approximation, which states that the Lorentz force on a particle vanishes in the fluid rest-frame: $u_\mu F^{\mu\nu} = 0$. There are still Lorentz forces on the current-carriers (usually electrons), of course, because the electrons don't move precisely with the fluid velocity u^μ .

Next, conservation of energy-momentum:

$$\partial_t(\sqrt{-g}T^t{}_\nu) = -\partial_i(\sqrt{-g}T^i{}_\nu) + \sqrt{-g}T^\kappa{}_\lambda \Gamma^\lambda{}_{\nu\kappa} \quad (4)$$

where $T^{\mu\nu}$ is the stress-energy tensor for MHD:

$$T_{\mu\nu} = (\rho_o + u + p + \frac{b^2}{4\pi})u_\mu u_\nu + (p + \frac{b^2}{8\pi})g_{\mu\nu} - \frac{b_\mu b_\nu}{4\pi}. \quad (5)$$

The space components of this equation may be compared with the nonrelativistic momentum equation

$$\partial_t(\rho\mathbf{v}) = -\nabla \cdot \mathbf{T} - \rho\nabla\phi, \quad (6)$$

where the MHD stress tensor is

$$T_{ij} = \rho v_i v_j + (p + \frac{B^2}{8\pi})\delta_{ij} - \frac{B_i B_j}{4\pi}. \quad (7)$$

Notice that gravitational forces have changed from $\rho\nabla\phi$ to $T^\kappa_\lambda\Gamma^\lambda_{\nu\kappa}$, where Γ is the connection coefficient or Christoffel symbol. Comparing the space-space components of $T^{\mu\nu}$ with T_{ij} , the main new feature is the replacement of $\rho v_i v_j$ by $(\rho_o + u + p + b^2/(4\pi))u_\mu u_\nu$; this accounts for the inertia associated with the pressure, internal energy, and magnetic field.

The induction equation can be written in conservative form:

$$\partial_t(\sqrt{-g}B^i) = -\partial_j(\sqrt{-g}(u^j b^i - b^j u^i)) \quad (8)$$

$$\partial_t \mathbf{B} = \nabla \times (\mathbf{v} \times \mathbf{B}) = -\nabla(\mathbf{v}\mathbf{B} - \mathbf{B}\mathbf{v}) \quad (9)$$

where the nonrelativistic equation is below. Finally the last component of Maxwell's equations becomes the no-monopoles constraint:

$$\partial_i(\sqrt{-g}B^i) = 0 \quad \nabla \cdot \mathbf{B} = 0, \quad (10)$$

and again the usual nonrelativistic form is on the right. Together with an equation of state we now have a complete set of equations for GRMHD.

The linear modes of the GRMHD equations reduce to the usual slow, Alfvén, and fast modes of nonrelativistic MHD if $b^2/(\rho_o + u + p) \ll 1$ and if the wavelength is much less than the characteristic scale of the geometry, here $> GM/c^2$. In the rest frame of the fluid the Alfvén speed (squared) is $b^2/(b^2/c^2 + 4\pi(\rho_o + u + p))$, which clearly asymptotes to c^2 for large b^2 . In the limit that $b^2/(\rho_o + u + p) \gg 1$ the fluid terms in the stress-energy tensor may be neglected and one is left with the equations of degenerate, force-free electrodynamics (see, e.g., McKinney & Gammie 2004). In this limit the fast mode becomes a vacuum electromagnetic wave. This force-free limit turns out to be generically difficult for GRMHD codes to handle.

3.1. NUMERICAL METHODS

Many efforts have been made to implement GRMHD schemes. As of this writing we are aware of *general* relativistic schemes associated with Koide's group^{16,17} in Toyama, Hawley and DeVillier's group¹⁸ in Virginia, our group¹⁹ in Illinois, and Komissarov²⁰ in Leeds. Each group has taken rather different numerical approaches; our group decided to implement a conservative scheme using a simple, robust approximate Riemann solver.

Our numerical scheme is described in reproducible detail in Ref. 19. Briefly, we use a conservative, Godunov type scheme with a simple approximate Riemann solver—either the local Lax-Friedrichs scheme, or the HLLC solver. The method is second order in space and time on smooth

flows. A divergence free field is maintained using the zone-centered constrained transport scheme suggested by Tóth²¹; this modification of Evans & Hawley’s²² constrained transport applies a smoothing operator to the fluxes used in the magnetic field evolution to preserve a particular numerical representation of $\nabla \cdot \mathbf{B} = 0$.

Conservative schemes are complicated in relativistic MHD by the nonlinear relationship between the conserved variables, which appear under the time derivative and are actually stepped forward by the code (e.g. momentum and energy density), and the primitive variables from which the fluxes are calculated (e.g. density, internal energy, and velocity). Our code (HARM¹⁹) uses the primitive variables ρ_o , u , B^i , and $\tilde{u}^i = u^i + \gamma\beta^i/\alpha$, where $\gamma^2 = 1 + g_{ij}\tilde{u}^i\tilde{u}^j$, $\beta^i = g^{ti}\alpha^2$ is the “shift,” and $\alpha^2 = -1/g^{tt}$ is the “lapse.” The numerical advantage of \tilde{u} is that it ranges from $-\infty$ to ∞ , and so it is more difficult for a truncation error to push the fluid state outside the lightcone (with disastrous consequences!).

As an example of the nonlinear relation between primitive and conserved variables, consider the rest-mass density in the coordinate frame: $\sqrt{-g}\rho_o u^t$. The fluid-frame rest-mass density cannot be easily extracted from this because it depends also on $u^t = \gamma/\alpha = \sqrt{1 + g_{ij}\tilde{u}^i\tilde{u}^j}/\alpha$.

One must therefore numerically invert from conserved to primitive variables once or even twice per timestep; by contrast, the inversion procedure is trivial and analytic in nonrelativistic MHD. The inversion can be broken into two pieces: the magnetic fields are trivially obtained from the conserved variables, but the five fluid variables ρ_o , u , and \tilde{u}^i are more difficult. Our standard method is to invert the associated set of five nonlinear equations directly using a multidimensional Newton-Raphson scheme. Usually only a few iterations are required because the fluid variables do not change much over a timestep, so good guesses are available from the last timestep. Nevertheless the variable inversion is one of the most expensive pieces of any conservative relativistic fluid scheme, in our case taking as much as 70% of the total CPU cycles, the exact percentage depending on the difficulty of the problem.

We are experimenting with a more efficient method that is a general relativistic extension of Del Zanna & Bucciantini’s scheme²³ for special relativistic MHD²⁴. This scheme involves the numerical solution of only a single nonlinear equation, so it is faster. In some situations, however, it may be less robust.

We have spent considerable effort testing HARM. This is difficult because of the paucity of exact results— especially exact time-dependent re-

sults. A suite of test problems and results are described in Gammie et al.¹⁹ and De Villiers & Hawley¹⁸.

One particularly useful test problem is the “inflow solution”²⁵. This is a one dimensional problem which is meant to describe nearly equatorial flow from the innermost stable circular orbit to the event horizon. The flow is assumed to be cold (zero pressure) and to be attached to circular geodesics at the ISCO. The magnetic field and velocity field are purely radial in the poloidal plane (but the toroidal components are nonzero); this *assumes* a solution to the trans-field force balance equation. This model is analogous to the old Weber-Davis²⁶ model for the solar wind, only it describes flow inward from the disk instead of outward from the solar equator. The inflow solution is a good test problem because it exercises many of the relevant terms in the equations of motion, including both the “gravitomagnetic” terms from the geometry *and* nontrivial magnetic stresses.

Figure 2 shows a convergence plot for the nontrivial dependent variables in one series of test calculations using the equatorial inflow solution. The number of grid points N between the ISCO and the horizon were varied and, as expected, the numerical solution converges to the exact solution as N^{-2} .

The inflow test results and results from Komissarov’s nonlinear wave tests, time-dependent linear wave tests, Bondi flow, magnetized Bondi flow, nonrelativistic Orszag-Tang vortex tests, and other tests, give us confidence that we are correctly integrating the equations of ideal GRMHD. The challenge now is to apply this to problems of astrophysical interest.

4. NUMERICAL MODEL

Our standard numerical model begins with a Fishbone-Moncrief equilibrium torus around a black hole. Were there no magnetic fields present, this would be a stable equilibrium (in axisymmetry). But we introduce a weak poloidal magnetic field that follows isodensity contours, and this is enough to make the disk vulnerable to the magnetorotational instability¹³. We introduce some small perturbations to get things going, and then integrate for $2000GM/c$, or about 7.5 orbital periods at our fiducial torus’s pressure maximum. The perturbations grow exponentially, the torus becomes turbulent, and matter begins to fall into the black hole.

Figure 3 shows the poloidal magnetic field configuration in the initial conditions and at the end of the evolution. The field in the disk becomes tangled on a scale of order the disk scale height. Some poloidal field threads

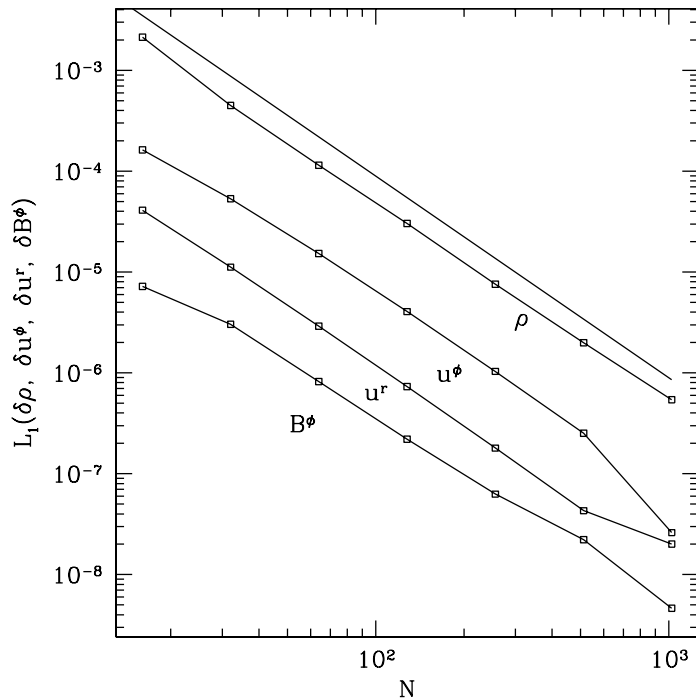


Figure 2. Convergence for the magnetized equatorial inflow solution. The spacetime has $a/M = 0.5$ and the dimensionless field strength $F_{\theta\phi} = 0.5$.

the hole in an ordered fashion, emerging in a near-monopole geometry near the poles.

The structure of the quasi-steady turbulent state that runs from a few hundred M to the end of the integration is summarized in Figure 4. Near the poles the field is ordered and almost radial, and the density and pressure are so low that the field dominates the energy density. At the boundary of this region (the “funnel”) there is a weak outflow with an asymptotic Lorentz factor of 1.5. This outflow is under a numerical cloud, however, because when our density “floor” is lowered the flow accelerates (we cannot reach a converged state because at very low values of the floor the integration fails). At still lower latitude is a “coronal” region with approximately thermal field, and near the equator is a centrifugally supported disk with subthermal field. The plunging region is rather similar to the disk in density

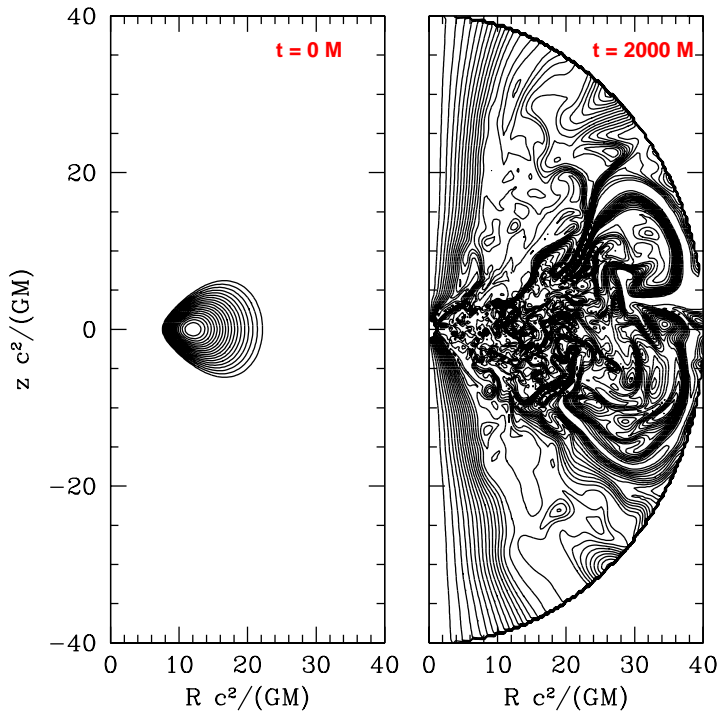


Figure 3. Poloidal magnetic field in the initial conditions and at $t = 2000GM/c$.

and magnetic field strength, although the flow is more ordered.

5. COMPARISON TO BLANDFORD-ZNAJEK MODEL

In our numerical models the funnel region has $b^2/\rho \gg 1$, an ordered field, and relatively little time variability. It may therefore be well described by the Blandford-Znajek force free model.

A direct check of the magnitude of the departures from a force-free configuration (the $\mathbf{J} \times \mathbf{B}$ force, or $J_\mu F^{\mu\nu}$) indicates that the funnel is very nearly force-free²⁷.

One can check other quantitative aspects of the BZ model. Figure 5 compares the electromagnetic component of the radial energy flux $-T_t^r = F_E^{(EM)}$ on the event horizon in the BZ model and a low-spin ($a/M = 0.5$) integration. The BZ model has one parameter here, the field strength at the pole, and this is set by requiring that it match the time-averaged value

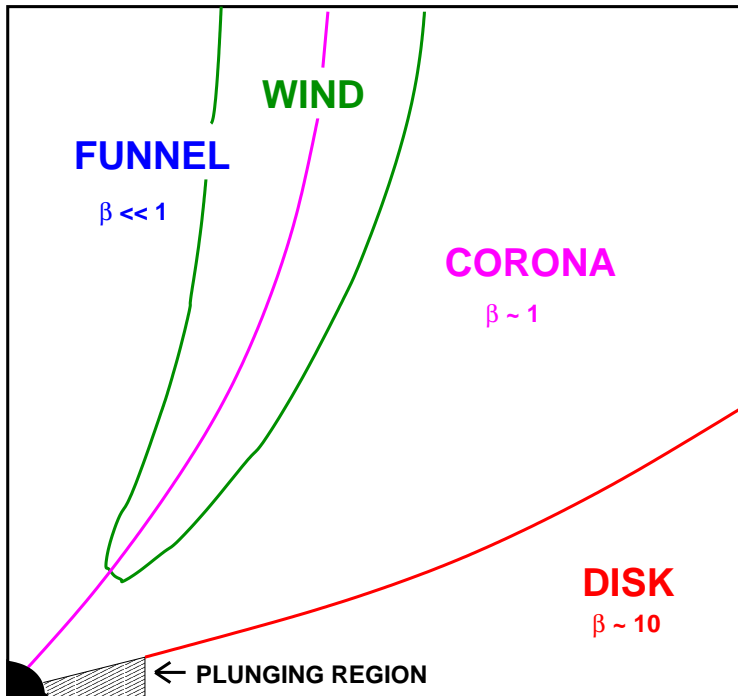


Figure 4. Mean structure of the time-dependent solution.

in the simulation. The BZ model matches quite well over the entire range where the plasma is close to force free.

Another prediction of the BZ model is that a quantity ω , usually called the rotation frequency of the magnetic field (which in MHD is equal to the plasma rotation frequency only where the poloidal velocity vanishes), should be $1/2$ the black hole rotation frequency $a/(2r_h)$, where $r_h = (GM/c^2)(1 + \sqrt{1 - a^2})$ is the horizon radius. An analysis of the time-averaged simulation data shows that ω is constant along field lines and within 10% of the expected value.

6. ANGULAR MOMENTUM ACCRETION

As already mentioned, the thin disk predicts the angular momentum per baryon of accreted material: it should be equal to the specific angular momentum of a particle on the ISCO. There are reasons to doubt that this should apply in a self-consistent MHD model. After all, one expects that

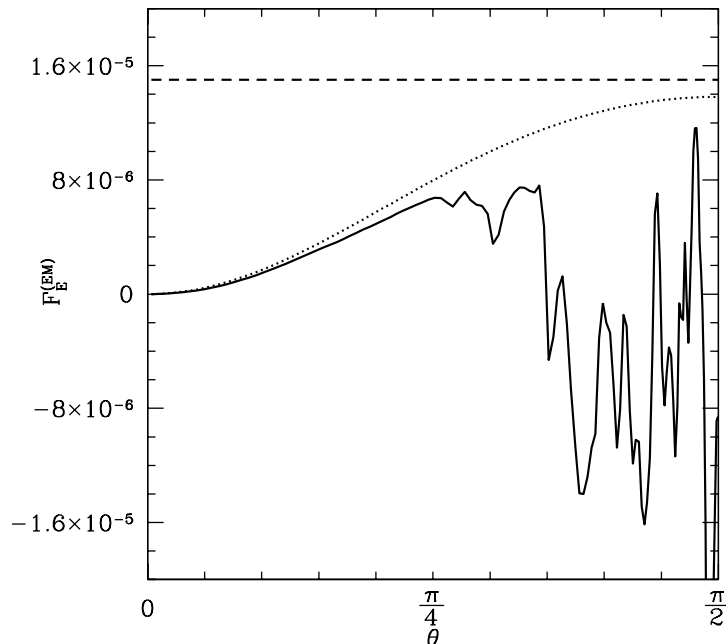


Figure 5. Comparison of the Blandford-Znajek electromagnetic energy flux at the event horizon (dotted line) with the numerical time and hemisphere averaged value (solid line).

any magnetic field will connect the plasma in the plunging region back to the disk. This field will be sheared by the inflow and an outward angular momentum flux will be set up (this point was also made in Thorne¹¹, quoting J. M. Bardeen). This possibility is realized in the inflow model of Gammie²⁵, where even a modest magnetic field sharply reduces the angular momentum of accreted material. But the inflow model is steady, cold, and assumes a particular boundary condition at the ISCO. What happens in a self-consistent dynamical calculation?

Figure 6 shows the rest-mass accretion rate \dot{M}_o , and the specific angular momentum (\dot{L}/\dot{M}_o) and energy (\dot{E}/\dot{M}_o) of the accreted material as a function of time in our fiducial calculation.

The dashed line in the figure indicates the time average; the dotted line indicates the prediction of the thin disk model (for $a/M = 0.938$).

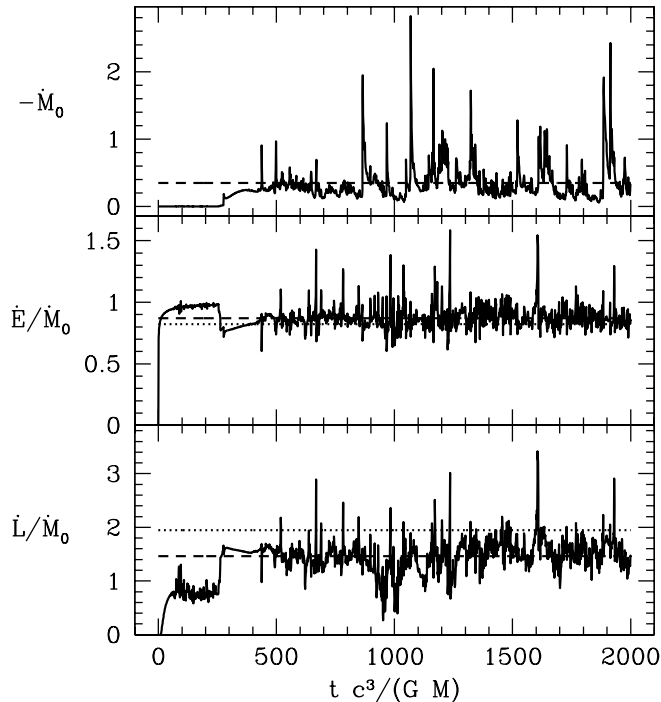


Figure 6. The rest-mass accretion rate \dot{M}_o , and the specific angular momentum (\dot{L}/\dot{M}_o) and energy (\dot{E}/\dot{M}_o) of the accreted material as a function of time in our fiducial calculation.

Evidently the angular momentum per baryon accreted is smaller than thin disk for this model.

We now consider a series of model with varying a/M but constant disk thickness. In each model we measure the dimensionless spin-up parameter $s = d(a/M)/dt(M/\dot{M}_o)$. If $s > 0$ the black hole is spinning up. Figure 7 shows the result of this survey.

Evidently for $a/M > 0.93$ the black hole is spinning down; the black hole reaches spin equilibrium at $a/M \simeq 0.93$ (where $\epsilon = 17\%$). This is similar in spirit to Thorne's¹¹ calculation, except that his radiating thin disk model reached spin equilibrium at $a/M = 0.998$ (where $\epsilon = 32\%$).

A few caveats: the models we've studied here are thick disks, which in α disk theory correspond to near-Eddington accretion. At lower accretion rates, if the disk can cool efficiently, the disk is thinner and the angular

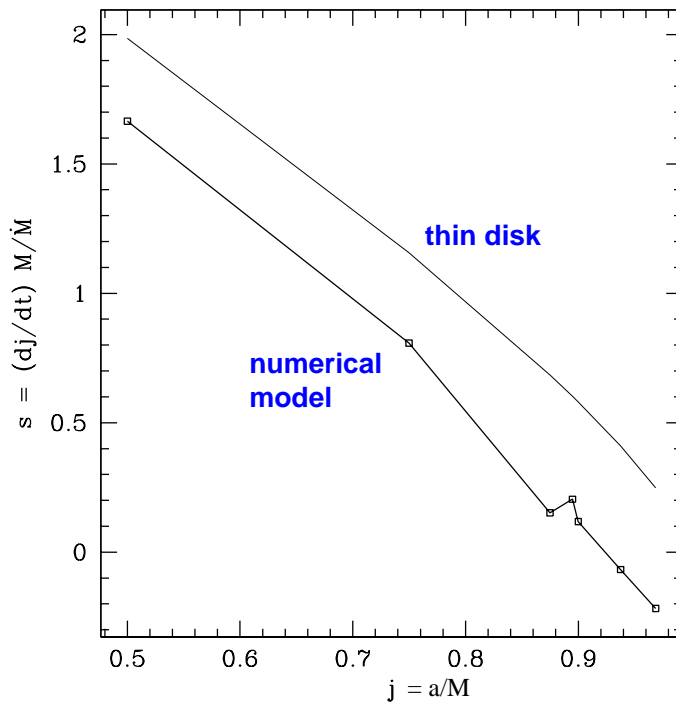


Figure 7. Dimensionless spin-up parameter vs. a/M at constant H/R .

momentum accretion rate may be closer to the thin disk predictions (as argued by Afshordi & Paczynski²⁸). Thin disks have not yet been studied numerically because when H/R is small many grid zones are required if both the radial and vertical directions are to be equally well resolved. Another caveat is that we've not included any of the effects of the radiation field, either in the cooling or the dynamics.

7. ENERGY ACCRETION

Next, we can look at the energy per baryon of accreted material. This is related to nominal luminosity of the black hole accretion flow, since any rest-mass energy that doesn't go into the hole must be carried away as high frequency electromagnetic radiation, low frequency plasma modes, a steady Poynting flux, or fluid energy flux in, e.g., an outflow. This allows us to define a nominal efficiency $\epsilon = 1 - \dot{E}/\dot{M}_o$.

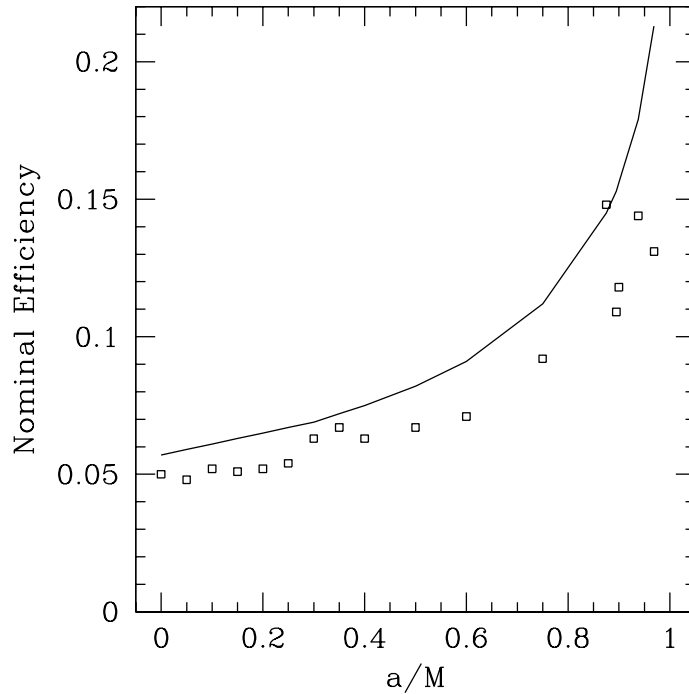


Figure 8. Nominal efficiency as a function of a/M . The points show the numerical data in a series of runs with H/R constant, and the solid line shows the thin disk prediction.

Figure 8 shows the nominal efficiency in the same series of simulations as used for figure 7. Evidently the efficiency is remarkably close to the thin disk efficiency— or even a little less— contrary to what one might anticipate from the inflow solution model. This is a bit of a surprise: why should the thin disk predictions be so close for the energy and not for the angular momentum? Perhaps the flow adjusts conditions at the ISCO self-consistently to cancel out any “extra” energy flux from the plunging region.

The energy flux on the event horizon can be split into electromagnetic and matter parts. For sufficiently rapidly rotating holes the electromagnetic part is directed outward. One might call this the Blandford-Znajek flux. The flux density is largest at temperate latitudes on the hole, but is positive all the way to the poles, so this Poynting flux might propagate through the near-empty funnel region and emerge at large distance in the form of high

quality (energy) photons.

Is the BZ flux energetically significant? Figure 9 shows \tilde{L} , the ratio of the BZ flux to the nominal accretion luminosity $\dot{M}_o - \dot{E}$. Evidently the BZ flux is a rapidly increasing function of a/M , and is about 1/4 of the nominal accretion luminosity for the most rapidly rotating models we have studied. Notice that this plot shows only our standard series of models, which all begin with the magnetic field entirely inside the initial torus. Numerical experiments beginning with a torus with net dipole moment evolve rather differently and show larger \tilde{L} , although even for these models $\dot{E}/\dot{M}_o > 0$, i.e. there is no net energy extraction.

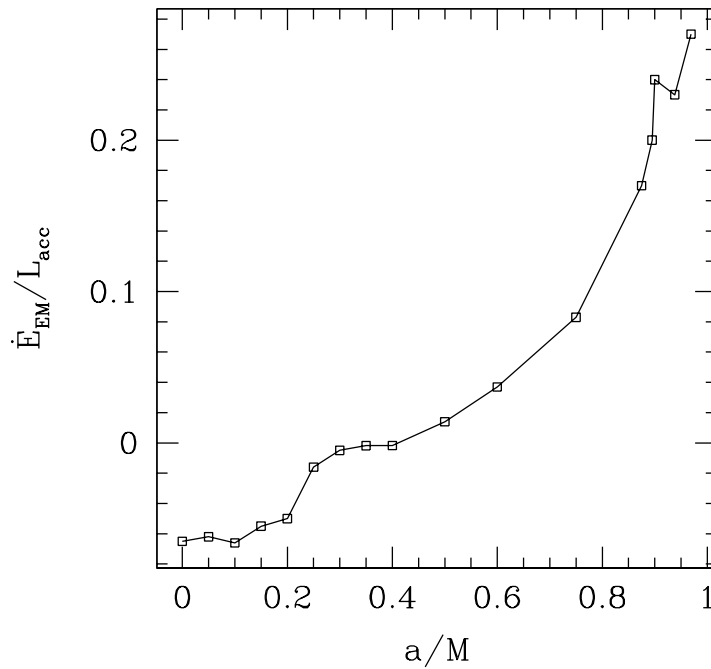


Figure 9. Ratio of the BZ flux (electromagnetic flux on the event horizon) to the nominal accretion luminosity as a function of a/M .

8. CONCLUSION

Much has been accomplished in recent years in setting the theory of black hole accretion flows on a firmer dynamical footing. Nonradiative, ideal models indicate that the flow has a disk-corona-funnel structure, as shown in Figure 4. Certain possible flow configurations that had been speculated on earlier, such as field lines that thread the disk and the black hole at high latitude, are not seen. Proper dynamical treatment of the magnetic field in thick (hot) accretion flows leads to lower specific angular momentum of the accreted material, because fields are able to connect plasma in the plunging region to plasma in the disk, transferring angular momentum outwards. This suggests that black holes will reach spin equilibrium at $a/M \sim 0.93$, much less than the 0.998 of Thorne¹¹.

In our numerical experiments the energy accreted per baryon is, somewhat surprisingly, very close to the thin disk value. This is contrary to expectations, based on steady MHD flow models^{25,29,30}, that the energy per baryon should be *lower* than thin disk, that is, that the accretion efficiency should be higher. This has not been born out by our (admittedly nonradiative) thick disk experiments. The reason for this discrepancy likely lies with the boundary conditions used in the steady MHD flow models, which use a zero-temperature approximation and assume (consistent with this) that the flow is anchored to geodesic flow on the innermost stable circular orbit.

Much remains to be done. The most glaring omission, as it were, from the current round of numerical models is the absence of any interaction of the plasma with the radiation field. This is a difficult problem to treat numerically, although optically thick and optically thin limits may be accessible within the next few years. There is also the interesting question of how the disk might interact with the gravitational field, a point of possible importance in understanding the outcome of neutron star-neutron star mergers and core collapse supernovae. Recent advances in numerical relativity should make this question accessible within a few years as well.

Acknowledgments

This work was supported in part by a NASA GSRP Fellowship Grant S01-GSRP-044 to JCM, and NSF Grants AST-0093091 and PHY 02-05155. Computations were done in part on `platinum.ncsa.uiuc.edu`.

References

1. Bardeen, J. M., *Nature* **226**, 64 (1970).
2. Pringle, J. E. & Rees, M. J. *A&A* **21**, 1 (1972).
3. Lynden-Bell, D. & Pringle, J. E. *MNRAS* **168**, **603** (1974).
4. Shakura, N. I. & Sunyaev, R. A. *A&A* **24**, 337 (1973).
5. Novikov I. D., Thorne K. S., In C. DeWitt and B. DeWitt (eds.) *Black Holes*. Gordon & Breach, New York, p. 343 (1973).
6. Blandford, R. D. & Znajek, R. L. , *MNRAS* **179**, **433** (1977).
7. Bardeen, J. M. & Petterson, J. A. , *ApJ* **195**, L65 (1975).
8. Kumar, S. & Pringle, J. E. *MNRAS* **213**, 435 (1985).
9. Scheuer, P. A. G. & Feiler, R. *MNRAS* **282**, 291 (1996).
10. Bardeen, J. M., Press, W. H., & Teukolsky, S. A. *ApJ* **178**, 347 (1972).
11. Thorne, K. S. *ApJ* **191**, 507 (1974).
12. Komissarov, S. S. *MNRAS* **303**, 343 (1999).
13. Balbus, S. A. & Hawley, J. F. *ApJ* **376**, 214 (1991).
14. Lichnerowicz, A. *Relativistic Hydrodynamics and Magnetohydrodynamics*, New York: Benjamin (1967).
15. Anile, A.M., *Relativistic Fluids and Magneto-fluids*, (New York: Cambridge Univ. Press) (1989).
16. Koide, S., Shibata, K., & Kudoh, T. *ApJ* **522**, 727 (1999).
17. Koide, S. *Phys. Rev. D* **67**, 104010 (2003)
18. De Villiers, J. & Hawley, J. F. *ApJ* **589**, 458 (2003).
19. Gammie, C. F., McKinney, J. C., & Tóth, G. , *ApJ* **589**, 444 (2003).
20. Komissarov, S. S. *MNRAS* **350**, 1431 (2004).
21. Tóth, G. *Journal of Computational Physics*, **161**, 605 (2000).
22. Evans, C. R. & Hawley, J. F. *ApJ* **332**, 659 (1988).
23. Del Zanna, L. & Bucciantini, N. *A&A* **390**, 1177 (2002).
24. Noble, S. Del Zanna, L. & Gammie, C. F., in preparation (2004).
25. Gammie, C. F. *ApJ* **522**, L57 (1999).
26. Weber, E. J. & Davis, L. J. *ApJ* **148**, 217 (1967).
27. McKinney, J.C. & Gammie, C.F. *ApJ*, in press (2004).
28. Afshordi, N. & Paczyński, B. *ApJ* **592**, 354 (2003).
29. Krolik, J. H. *ApJ* **515**, L73 (1999).
30. Agol, E. & Krolik, J. H. *ApJ*, **528**, 161 (2000).